Insulator-quantum Hall transitionin monolayer epitaxial graphene

Lung-I Huang[ab], Yanfei Yang[ac], Randolph E. Elmquist[a],
Shun-Tsung Lo[*d], Fan-Hung Liu[d], and Chi-Te Liang[*bde]

[a]*National Institute of Standards and Technology (NIST), Gaithersburg, MD 20899, USA*
[b]*Department of Physics, National Taiwan University, Taipei 106, Taiwan*
[c]*Department of Physics, Georgetown University, Washington, DC 20057, USA*
[d]*Graduate Institute of Applied Physics, National Taiwan University, Taipei 106, Taiwan*
[e]*Geballe Laboratory for Advanced Materials (GLAM), Stanford University, Stanford, CA 94305, USA*

We report on magneto-transport measurements on low-density, large-area monolayer epitaxial graphene devices grown on SiC. We observe temperature (T)-independent crossing points in the longitudinal resistivity ρ_{xx}, which are signatures of the insulator-quantum Hall (I-QH) transition, in all three devices. Upon converting the raw data into longitudinal and Hall conductivities σ_{xx} and σ_{xy}, in the most disordered device, we observed T-driven flow diagram approximated by the semi-circle law as well as the T-independent point in σ_{xy} near e^2/h. We discuss our experimental results in the context of the evolution of the zero-energy Landau level at low magnetic fields B. We also compare the observed strongly insulating behaviour with metallic behaviour and the absence of the I-QH transition in graphene on SiO_2 prepared by mechanical exfoliation.

1. Introduction

When a strong magnetic field B is applied perpendicular to the plane of monolayer graphene,[1-3] Landau quantization results in a series of Landau levels whose energies are given by[4]

$$E_{\mathrm{N}} = \mathrm{sgn}(N)\sqrt{2\hbar v_{\mathrm{F}}^2 eB|N|}, \quad (1)$$

where N, $\hbar$, e, v_F are an integer, reduced Planck constant, electronic charge and Fermi velocity, respectively. According to Eq. (1), the energy of the $N = 0$ Landau level (LL) is always zero and thus is independent of B. Such a zeroth LL, which is shared equally by electrons and holes with degeneracy of four, is unique in graphene and has no counterparts in any semiconductor-based two-dimensional (2D) systems. It is worth mentioning that graphene on SiO_2 can form electron hole puddles[5] due to interactions between graphene and its substrate. Such an effect can greatly modify the electronic properties of graphene. Therefore the B-independent zero-energy LL (Eq. (1)) should be considered as the theoretical limit of non-interacting, ideal graphene system.

Although in most cases, transport in graphene on SiO_2 prepared by mechanical exfoliation shows metallic behaviour or a very weak T dependence,[1, 2] insulating behaviour in the sense that the resistivity decreases with increasing T can appear in suspended graphene on SiO_2,[6] and in graphene on hexagonal boron nitride (h-BN) when sublattice symmetry is broken.[7] It is also known that h-BN can substantially increase the mobility of graphene device and the induced sublattice symmetry breaking allows the observation of Zeeman spin degeneracy lifting of the LLs in the presence of a magnetic field.[8,9] Interestingly, recent experiments show very low conductivity near the charge neutrality point for monolayer graphene on boron nitride

with a suspended top gate[7] and for monolayer epitaxial graphene (EG) with a point-like constriction caused by bilayer patches.[7] Such important results on monolayer graphene suggest further studies are required and may be related to the possible splitting of the zeroth LL (ref. 11) at low *B*. Moreover, insulating behaviour and a temperature-independent point in the measured resistivity are observed in a disordered monolayer EG device.[12] Here, we address the two aforementioned fundamental issues: the fate of the zero-energy LL at low fields and the insulating behaviour in disordered graphene. In the most disordered EG device, we observe a well-defined *T*-independent point in the measured Hall conductivity σ_{xy} and the appearance of a semicircle relation in the *T*-driven flow diagram.[13] Such results are in sharp contrast to the theoretical understanding of the zero-energy LL which is believed to be *B*-independent. Moreover, our data provide a thorough understanding of the low-field insulator-quantum Hall (I-QH) transition in disordered EG as well as the metallic-like behaviour in graphene on SiO_2.

2. Experimental section

Our EG devices were fabricated utilizing a clean lithography process[14] that leaves the surface free of resist residues. After the fabrication process, doping occurs due to or initiated by chemical etching of the protective layer and exposure to air. We have engineered the carrier density as low as $n \approx 10^{15}$ m^{-2}. Here, the exposed Si atoms in the SiC(0001) lattice form partial covalent bonds to carbon atoms in the lower graphene layer (buffer layer), and only the top layer is conducting. Si-C covalent bonds and defects such as interfacial dangling bonds affect the electrical environment of the graphene sheet and graphene-substrate coupling may break its sublattice symmetry.[15] Low carrier density is known to reduce the screening of Coulomb

potential fluctuations, and therefore enhances the SiC substrate effect on the conducting graphene sheet.

Large-area EG devices are suitable for studies of QH transitions and insulating behaviour since the long-range effects of increasing disorder may be hidden by local or size-dependent phenomena for small samples.[16] Moreover, in EG grown on SiC,[17, 18] E_F can be pinned to the localized states[19] such that the $\nu = 2$ QH plateau extends from a low field (~ 1 T) to exceptionally high values (30 T),[20] making EG an ideal system for studying an isolated low-field QH transition, although no such high-field transition has been reported. A possible reason for this is the reservoir model responsible for the long $\nu = 2$ QH plateau[19] so that one does not observe the high-field insulating state. Measurements on large-area (0.6 mm × 0.1 mm) devices were made in a perpendicular magnetic field up to 9 T in a variable-temperature cryostat using standard low-frequency lock-in techniques.

3. Results and discussion

Figure 1a-c show the atomic force microscope (AFM) images taken on the three samples (EG1, EG2 and EG3) which were studied in this work. Although both samples were grown at the same temperature of 1900 ^{o}C, the surface roughness of EG1 appears to be lower than that of EG2. As will be shown later, although the surface roughness of EG3 is slightly lower than that of EG2, the resistivity of EG3 device is higher than that of EG2 (and that of EG1). One possible reason is that the growth temperature of EG3 (1800 ^{o}C) is lower than those of EG1 and EG2, rendering EG3 the most disordered among the three devices which will be described later.

The longitudinal and Hall resistivities (ρ_{xx} and ρ_{xy}) for EG1, EG2, and EG3 at various T are plotted in Figs. 2a-c. The low-T resistivity of EG1 is nearly two times lower than that of EG2. However, the mobility of EG1 is lower than that of EG2. Therefore it is not possible to tell whether the level of disorder in EG1 or in EG2 is higher. Nevertheless, since both the mobility and zero-field conductivity of EG3 is the lowest among the three devices, we believe that EG3 is the most disordered sample. We can immediately see the T-independent points in ρ_{xx} at crossing fields B_c in all three samples. For $B < B_c$, the device behaves as an insulator in the sense that ρ_{xx} decreases with increasing T.[21] For $B > B_c$, the device shows QH-like behaviour and ρ_{xx} increases with increasing T.[21-24] Our results show characteristics of the insulator to $\nu = 2$ QH transition observed in disordered 2D systems.[20-22] Like other disordered 2D systems, localization and interaction effects are observed in our devices (see Supporting Information).

To further study the observed I-QH transition,[12] we plot σ_{xx} and σ_{xy} for EG1, EG2 and EG3 in Figs. 3a-c. Interestingly, a clear T-independent crossing point in σ_{xy} develops near e^2/h for EG2 and EG3. In the scaling theory of the QH effect, values of σ_{xy} that are half multiples of e^2/h (per spin) behave as unstable points under renormalization.[21] Therefore the observed crossing point near e^2/h suggests a delocalization/localization process occurs when the zeroth LL passes *upwards* through E_F when B is decreased.[22]

A T-driven flow diagram in the (σ_{xy}, σ_{xx}) plane can be used to study the physics of localization processes in 2D systems.[25,26] A field-induced transition involves a transition between two fixed points in this diagram, with a sudden increase and a similar decrease in σ_{xx} once the LL is emptied or filled. It has been experimentally

verified that this transition traces out a semicircle[25] in the (σ_{xy}, σ_{xx}) plane and for systems with a single conduction channel the semicircle represents a critical boundary for the QH state. The semicircle is centered at (0, e^2/h) and follows $(\sigma_{xx})^2 + (\sigma_{xy} - e^2/h)^2 = (e^2/h)^2$, where the transition to the $\nu = 2$ QH state occurs.

Figures 4a and 4b show that samples EG1 and EG2 develop robust $\nu = 2$ QH characteristics to the right of the semicircle ($\sigma_{xy} > e^2/h$) at fields $B \approx 1$ T, and approach the limiting point of the QH state at ($2e^2/h$, 0). Conductivity data is given in Fig. 4 for all three EG samples with arrows showing *T*-driven flow superimposed at a series of fixed *B*. For a given sample, results at constant magnetic field strength that follow a vertical *T*-driven flow line corresponds to a critical field denoted by B_c^{σ} identified as a crossing point of constant conductivity σ_{xy}. Similar curved arrows show how flow divides along the critical boundary of the QH state, shown by a dotted semicircle, starting at an unstable point indicated by a black dot. EG1 avoids the critical boundary with high conductivity ($\sigma_{xx} \approx 4e^2/h$) at low fields, and the vertical flow line occurs at $\sigma_{xy} < e^2/h$. Vertical *T*-driven flow arrows in Figs. 4b and 4c show that the crossing magnetic field B_c^{σ} occurs close to $\sigma_{xy} = e^2/h$ for both EG2 and EG3, while the magnitude of σ_{xx} decreases from $\sigma_{xx} \approx 2e^2/h$ to $\sigma_{xx} \approx e^2/h$. Thus, we can characterize the *T*-driven flow for increasing disorder strength in our samples by vertical flow along $\sigma_{xy} = e^2/h$, the line that points toward the center of the $\nu = 2$ QH semicircle. Elsewhere the flow diverges from verticality especially near the semi-circle boundary, as clearly seen for sample EG3, where flow lines become nearly tangent to the semicircle.

Based on the floating up picture,[27, 28] Kivelson, Lee, and Zhang have proposed the global phase diagram (GPD) which describes possible phase transitions in a 2D

system.[29] When the spin degeneracy is considered, for a strongly disordered 2D system in which the spin-splitting is not well-resolved, the only I-QH transition is the 0-2 transition, where the numbers 0 and 2 correspond to the insulating phase and the v = 2 QH state. This 0-2 transition and the 2-0 transition, from the QH state to the insulating regime, are equivalent within the GPD framework.[29] The establishment of the semicircle relation for the 0-2 transition requires that the lowest extended band continuously floats up above E_F with smaller B.[22, 23, 27-29] Experimenta evidence for the floating-up of the extended states in GaAs has been claimed[27]. On the other hand, at low magnetic fields, extended states can float up then merge in a Si 2D system[31]. It was pointed out that chaotic potentials and possible oscillation of the boundary between the metallic and insulating phases[32] can make the observation of the pronounced floating-up of the extended states not realizable.[33]

The semicircle-like flow lines obtained on EG3 appears to be in line with the levitation of the zeroth LL in disordered graphene, linking the observed insulating behaviour in EG3 at low fields to the zeroth Landau band floating up above.[27] However, without the ability to tune the carrier density to trace the crossing point in σ_{xy} in our case, we cannot confirm the floating-up of the extended states at low B. The semicircle law does not provide a good explanation for the transition in the cleaner devices EG1 and EG2. The possible origin is that their weak disorder prohibits the observation of the levitating Landau band. Moreover we found that the slope of σ_{xy} at B_c^{σ} scales with temperature following $T^{-\kappa}$ with κ = 0.21 and 0.36 for EG2 and EG3, respectively (see Fig. S7 in the Supporting Information). At such low-field transitions, the Zeeman splitting plays a minor role, preserving the spin degeneracy. Therefore the increase in κ can be attributed to the breaking of sublattice symmetry in the presence

of potential fluctuations, which may split the zeroth Landau band.[34] With the strongest disorder in EG3, the semicircle relation between σ_{xy} and σ_{xx} becomes apparent, linking out results with possibly *B*-dependent zeroth Landau band due to disorder.

For EG3, the *T*-independent crossing point in ρ_{xx} occurs at the filling factor $\nu_c = nh/(eB_c)$ of 0.6, which is in agreement with the recently reported value for the high-field levitation of the zeroth Landau band.[35] However for EG1 and EG2, it corresponds to ν_c = 16 and ν_c = 7, respectively, which is much higher than that for EG3. These values deviate from the prediction of plateau-to-plateau transition between the ν = 6 and ν = 2 QH state, suggesting that the transition in weakly disordered EG1 and EG2 does not result from the N = 1 Landau band passing through the Fermi energy with magnetic field. In addition, at zero magnetic field, we have estimated the width $\Gamma \approx \hbar/\tau$ of Landau level broadening due to disorder. The results are 23 meV, 24 meV, 76 meV for EG1, EG2, and EG3, respectively. However the Fermi energy lies at E_F = 49 meV, 35 meV, and 28 meV for EG1, EG2, and EG3. Interestingly, for EG3, E_F is smaller than the estimated Γ. This finding infers a narrowing of the zeroth Landau band, which is robust against some sorts of disorder[36] such that we can still observe the ν =2 quantum Hall character in highly disordered EG3. It is worthwhile noting that the finite size effect and the charge transfer from the buffer layer/SiC interface (which partially determines the carrier density in a QH state) to the graphene sheet[20] would modify the transitions. Moreover, since we have observed logarithmic temperature dependent Hall slope in all the devices due to interaction effects (see Fig. S4a in Supplementary Information), electron-electron interactions which are not considered within the global phase diagram may be regarded as perturbation/modification to the original floating-up picture.

It was shown that graphene-substrate-induced sublattice symmetry breaking coupled with charge disorder in epitaxial graphene layer can substantially modify the

transport properties of graphene.[37] We note that in graphene on h-BN, strongly insulating behaviour *solely* due to graphene-substrate related sublattice symmetry breaking is observed.[6] Interestingly, such an insulating phase makes a direct transition to the $\nu = 0$ state at an extremely low field ($B \sim 0.1$ T) without an intermediate transition to the $\nu = 2$ QH state,[7] in sharp contrast to our experiment. In our case, the mobility of EG3 is 20 times lower than that of the graphene on h-BN. The stronger disorder and the fact that our device is not exactly at the Dirac point should inhibit the formation of the $\nu = 0$ state as supported by no sign of the $\nu = 0$ plateau in σ_{xy}. Therefore although insulating behaviour can be observed in both graphene on h-BN and disordered EG, we observe a transition from the insulating phase to the $\nu = 2$ QH state *as well as* the semi-circle-like *T*-driven flow diagram, in line with floating up of the $N = 0$ electron LL due to stronger disorder compared with that of Amet *et al.*[6] Our results, together with the pioneering work of Amet *et al.* suggest that sublattice symmetry breaking plays an important role in the observed insulating behaviour in graphene subject to the environment effect. The strength of disorder, however, determines the allowable transition between the insulating state and the $\nu = 2$ QH state or the $\nu = 0$ state. It is worth mentioning that graphene on SiO_2 can form electron hole puddles[32] due to the interactions between graphene and its substrate. Such an effect can greatly modify the electronic properties of graphene. Moreover, h-BN can substantially increase the mobility of graphene device and cause sublattice symmetry breaking which allows the observation of Zeeman spin degeneracy lifting of the LLs in the presence of a magnetic field.[36, 37] We note that the *B*-independent zero-energy LL (Eq. (1)) should be considered as the theoretical limit of non-interacting, ideal graphene system.

The unique *B*-dependent carrier density in epitaxial graphene grown on SiC, which can be ascribed to the reservoir model, has a pronounced effect on the QH transition. We would like to point out that though such an effect is solely responsible for the extremely long $\nu = 2$ quantum Hall plateau, it should not significantly affect the low-field I-QH transition observed in our devices. The reason for this is that a good crossing point requires fixed carrier density in the system as previously observed in conventional semiconductor-based systems in which the carrier density is *B*-independent.[21-23] Moreover, in all the theoretical studies on the I-QH transition, the carrier density is assumed to be constant, independent of both temperature and magnetic field.[27-29] Therefore the reservoir model describing charge transfer between epitaxial graphene and the SiC substrate as a function of *B* (Ref. 16) should not play an important role in the observed low-field I-QH transition in the work of Pallecchi *et al.*[12] as well as in our devices.

4. Conclusions

In conclusion, we have reported magneto-transport measurements on low-density monolayer EG with various amount of disorder. *T*-independent crossing points are observed in all three samples. We have found that the observed *T*-independent point in ρ_{xx} survives after subtraction of the electron-electron interaction corrections (see Supporting Information), demonstrating that such crossing points are related to magnetic-field-induced delocalization/localization transitions. *T*-independent points in σ_{xy} can emerge, corresponding to the unstable points under renormalization in the scaling theory of the QH effect. Our results therefore suggest that σ_{xy}, rather than ρ_{xx}, is the more important physical quantity in the study of quantum Hall transitions. Most

importantly, in the most disordered device, we have observed *T*-driven flow lines approximated by the semi-circle law. Such results are in line with the fact that the zeroth LL is levitated for $B < B_c$ and can explain the insulating behaviour in our EG . In the future, we plan to work on a gated EG device in order to tune the effectively disorder and carrier density within the same sample so that the evolution of the crossing point in σ_{xy} as well as *T*-driven flow diagram can be used to probe the fate of the zero-energy LL in graphene-based systems.

Acknowledgments

This work was funded by the Ministry of Science and Technology (MOST), Taiwan. C.T.L. was supported by the MOST, Taiwan (grant numbers MOST 103-2918-I-002-028, MOST 103-2622-E-002 -031, MOST 104-2622-8-002 -003 and MOST 102-2119-M-002 -016 -MY3).

*E-mail: shuntsunglo@mail.ncku.edu.tw and ctliang@phys.ntu.edu.tw

References

1. K. S. Novoselov, A. K. Geim, S. V. Morozov, D. Jiang, Y. Zhang, S. V. Dubonos, I. V. Grigorieva and A. A. Firsov, *Science*, 2004, **306**, 666-669.
2. K. S. Novoselov, A. K. Geim, S. V. Morozov, D. Jiang, M. I. Katsnelson, I. V. Grigorieva, S. V. Dubonos and A. A. Firsov, *Nature*, 2005, **438**, 197-200.
3. Y. Zhang, Y.-W. Tan, H. L. Stormer and P. Kim, *Nature*, 2005, **438**, 201-204.
4. A. H. Castro Neto, F. Guinea, N. M. R. Peres, K. S. Novoselov and A. K. Geim, *Rev. Mod. Phys.*, 2009, **81**, 109-162.
5. J. Martin, N. Akerman, G. Ulbricht, T. Lohmann, J. H. Smet, K. von Klitzing and A. Yacoby, *Nat. Phys.*, 2008, **4**, 144-148.
6. K. I. Bolotin, K. J. Sikes, J. Hone, H. L. Stormer and P. Kim, *Phys. Rev. Lett.*, 2008, **101**, 096802.
7. F. Amet, J. R. Williams, K. Watanabe, T. Taniguchi and D. Goldhaber-Gordon, *Phys. Rev. Lett.*, 2013, **110**, 216601.
8. K. I. Bolotin, F. Ghahari, M. D. Shulman, H. L. Stormer and P. Kim, *Nature*, 2009, **462**, 196-199.
9. C. R. Dean, A. F. Young, P. Cadden-Zimansky, L. Wang, H. Ren, K. Watanabe, T. Taniguchi, P. Kim, J. Hone and K. L. Shepard, *Nat. Phys.*, 2011, **7**, 693-696.

10. C. Chua, M. Connolly, A. Lartsev, T. Yager, S. Lara-Avila, S. Kubatkin, S. Kopylov, V. Fal'ko, R. Yakimova, R. Pearce, T. J. B. M. Janssen, A. Tzalenchuk and C. G. Smith, *Nano Lett.*, 2014, **14**, 3369-3373.
11. A. J. M. Giesbers, L. A. Ponomarenko, K. S. Novoselov, A. K. Geim, M. I. Katsnelson, J. C. Maan and U. Zeitler, *Phys. Rev. B*, 2009, **80**, 201403.
12. E. Pallecchi, M. Ridene, D. Kazazis, F. Lafont, F. Schopfer, W. Poirier, M. O. Goerbig, D. Mailly and A. Ouerghi, *Sci. Rep.*, 2013, **3**, 1791.
13. M. Hilke, D. Shahar, S. H. Song, D. C. Tsui, Y. H. Xie and M. Shayegan, *Europhys. Lett.*, 1999, **46**, 775-779.
14. Y. Yang, L.-I. Huang, Y. Fukuyama, F.-H. Liu, M. A. Real, P. Barbara, C.-T. Liang, D. B. Newell and R. E. Elmquist, *Small*, 2015, **11**, 90-95.
15. S. Y. Zhou, G. H. Gweon, A. V. Fedorov, P. N. First, W. A. de Heer, D. H. Lee, F. Guinea, A. H. Castro Neto and A. Lanzara, *Nat. Mater.*, 2007, **6**, 770-775.
16. T. Nakajima, T. Ueda and S. Komiyama, *J. Phys. Soc. Jpn.*, 2007, **76**, 094703.
17. C. Berger, Z. Song, T. Li, X. Li, A. Y. Ogbazghi, R. Feng, Z. Dai, A. N. Marchenkov, E. H. Conrad, P. N. First and W. A. de Heer, *J. Phys. Chem. B*, 2004, **108**, 19912-19916.
18. C. Riedl, C. Coletti and U. Starke, *J. Phys. D: Appl. Phys.*, 2010, **43**, 374009.
19. T. J. B. M. Janssen, A. Tzalenchuk, R. Yakimova, S. Kubatkin, S. Lara-Avila, S. Kopylov and V. I. Fal'ko, *Phys. Rev. B*, 2011, **83**, 233402.
20. J. A. Alexander-Webber, A. M. R. Baker, T. J. B. M. Janssen, A. Tzalenchuk, S. Lara-Avila, S. Kubatkin, R. Yakimova, B. A. Piot, D. K. Maude and R. J. Nicholas, *Phys. Rev. Lett.*, 2013, **111**, 096601.
21. S. H. Song, D. Shahar, D. C. Tsui, Y. H. Xie and D. Monroe, *Phys. Rev. Lett.*, 1997, **78**, 2200-2203.
22. H. W. Jiang, C. E. Johnson, K. L. Wang and S. T. Hannahs, *Phys. Rev. Lett.*, 1993, **71**, 1439-1442.
23. R. J. F. Hughes, J. T. Nicholls, J. E. F. Frost, E. H. Linfield, M. Pepper, C. J. B. Ford, D. A. Ritchie, G. A. C. Jones, E. Kogan and M. Kaveh, *J. Phys.: Condens. Matter*, 1994, **6**, 4763.
24. T. Wang, K. P. Clark, G. F. Spencer, A. M. Mack and W. P. Kirk, *Phys. Rev. Lett.*, 1994, **72**, 709-712.
25. H. P. Wei, D. C. Tsui and A. M. M. Pruisken, *Phys. Rev. B*, 1986, **33**, 1488-1491.
26. C. P. Burgess and B. P. Dolan, *Phys. Rev. B*, 2007, **76**, 113406.
27. D. E. Khemelinskii, *Pis'maZh. Eksp. Teor. Fiz.*, 1983, **38**, 454 [*JETP Lett.*, 1983, **38**, 552].
28. R. B. Laughlin, *Phys. Rev. Lett.*, 1984, **52**, 2304-2304.

29. S. Kivelson, D.-H. Lee and S.-C. Zhang, *Phys. Rev. B*, 1992, **46**, 2223-2238.
30. I. Glozman, C. E. Johnson and H. W. Jiang, *Phys. Rev. Lett.*, 1995, **74**, 594-597.
31. A. A. Shashkin, G. V. Kravchenko, V. T. Dolgopolov, JETP Lett. 1993, **58**, 220-224; Pis'ma Zh. Eksp. Teor. Fiz. 1993, **58**, 215-219
32. G. M. Gusev, U. Gennser, X. Kleber, D. K. Maude, J. C. Portal, D. I. Lubyshev, P. Basmaji, M. De. P. A. Silva, J.C. Rossi, Yu.V. Nastaushev, Solid State Commun. 1996, **100**, 269-273.
33. V T Dolgopolov, Physics-Uspekhi, 2014, **57**, 105-127
34. F. Ortmann and S. Roche, *Phys. Rev. Lett.*, 2013, **110**, 086602.
35. L. Zhang, Y. Zhang, M. Khodas, T. Valla and I. A. Zaliznyak, *Phys. Rev. Lett.*, 2010, **105**, 046804.
36. A. J. M. Giesbers, U. Zeitler, M. I. Katsnelson, L. A. Ponomarenko, T. M. Mohiuddin and J. C. Maan, *Phys. Rev. Lett.*, 2007, **99**, 206803.
37. X. Peng and R. Ahuja, *Nano Lett.*, 2008, **8**, 4464-4468.

Figure Captions

Fig. 1 AFM images taken on (a) EG1, (b) EG2, and (c) EG3. Left: surface and right: phase measurements

Fig. 2 ρ_{xx} and ρ_{xy} at different temperatures T for (a) EG1, (b) EG2, and (c) EG3. The vertical arrows indicate the temperature increase: T = 2.52 K, 3.50 K, 4.25 K, 5.50 K, 7.00 K, 8.50 K, and 10.0 K for EG1; T = 2.60 K, 3.54 K, 4.55 K, 5.56 K, and 7.00 K for EG2; T = 4.45 K, 7 K, 10 K, 15 K, and 25 K for EG3.

Fig. 3 The directly converted conductivities, σ_{xx} and σ_{xy}, at different T for (a) EG1, (b) EG2, and (c) EG3. The vertical arrows indicate the temperature increase. The temperature points are the same as those given in the caption of Fig. 1 for each sample.

Fig. 4 Conductivity σ_{xx} plotted against σ_{xy} for (a) EG1, (b) EG2 and (c) EG3. The

dotted curves denote the theoretical prediction of semicircle σ_{xx}-σ_{xy} relation for the 0-2 transition. Each group of triangle markers connected by dashed lines denotes the data for the same magnetic field. The arrows indicate the flow line to the low temperature extreme at fixed magnetic fields. The black ones correspond to the flow at the observed crossing point B_c^{σ} in σ_{xy}.

(a)

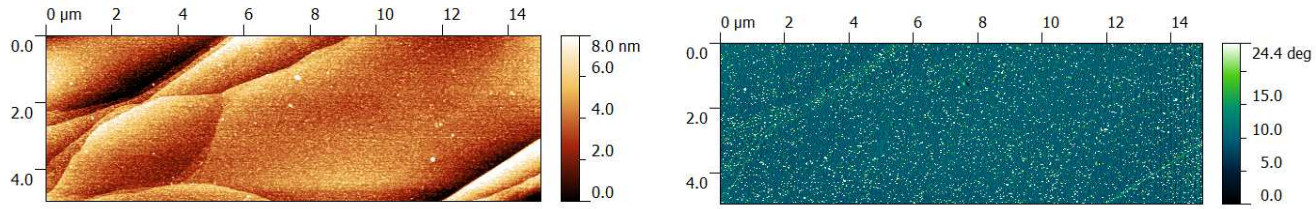
0 µm 2 4 6 8 10 12 14
0.0
2.0
4.0
8.0 nm
6.0
4.0
2.0
0.0
0 µm 2 4 6 8 10 12 14
0.0
2.0
4.0
24.4 deg
15.0
10.0
5.0
0.0

(b)

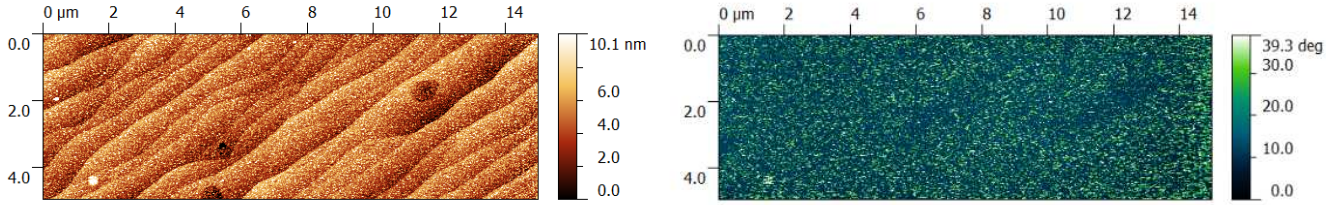
0 µm 2 4 6 8 10 12 14
0.0
2.0
4.0
10.1 nm
6.0
4.0
2.0
0.0
0 µm 2 4 6 8 10 12 14
0.0
2.0
4.0
39.3 deg
30.0
20.0
10.0
0.0

(c)

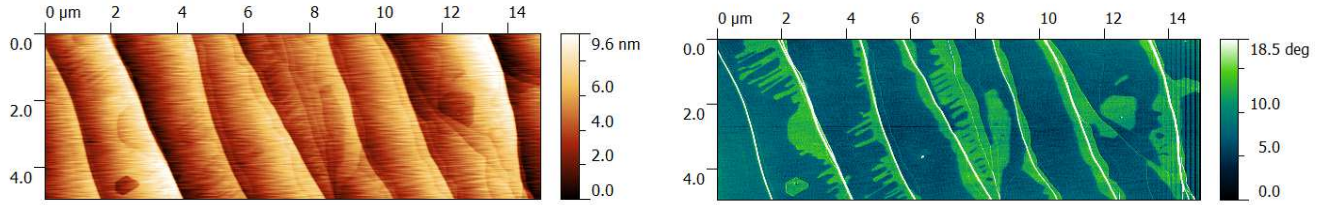
0 µm 2 4 6 8 10 12 14
0.0
2.0
4.0
9.6 nm
6.0
4.0
2.0
0.0
0 µm 2 4 6 8 10 12 14
0.0
2.0
4.0
18.5 deg
10.0
5.0
0.0

Figure 1

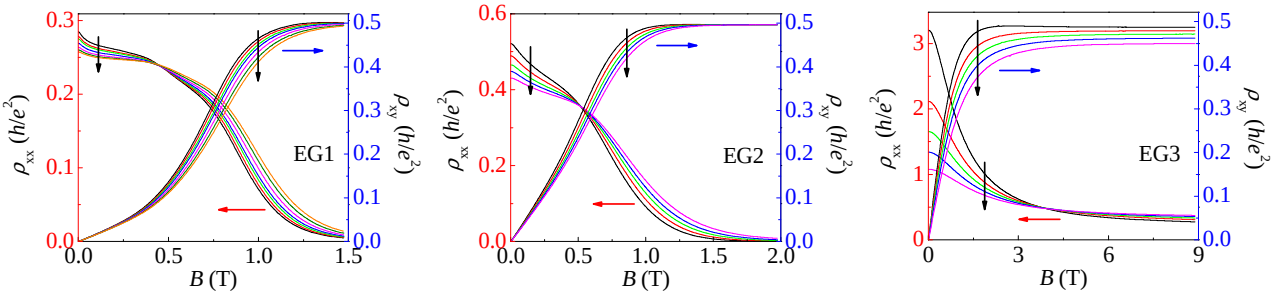

Figure 2

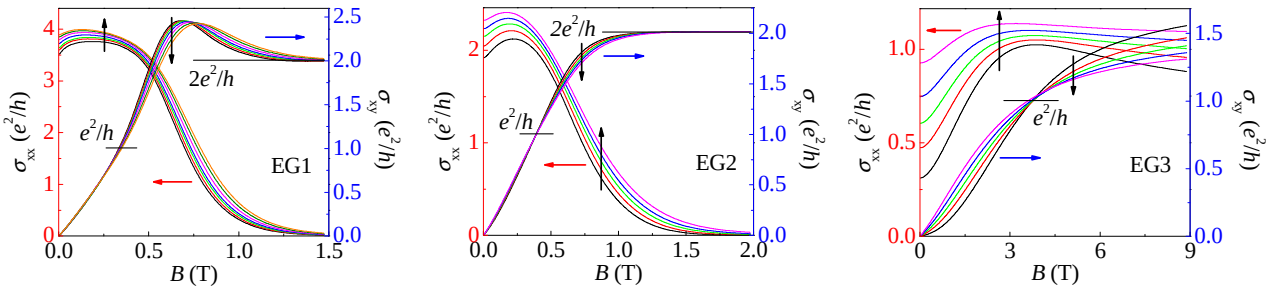

Figure 3

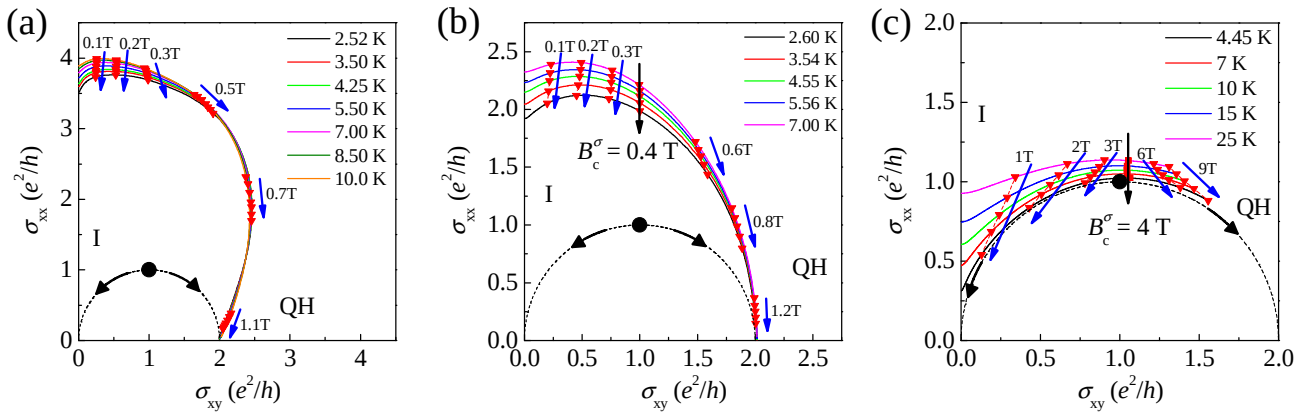
(a)
0.1T
0.2T
0.3T
0.5T
0.7T
1.1T
I
QH
2.52 K
3.50 K
4.25 K
5.50 K
7.00 K
8.50 K
10.0 K
σ_{xx} (e^2/h)
σ_{xy} (e^2/h)
(b)
0.1T
0.2T
0.3T
B_c^{σ} = 0.4 T
0.6T
0.8T
1.2T
I
QH
2.60 K
3.54 K
4.55 K
5.56 K
7.00 K
σ_{xx} (e^2/h)
σ_{xy} (e^2/h)
(c)
I
1T
2T
3T
6T
9T
B_c^{σ} = 4 T
QH
4.45 K
7 K
10 K
15 K
25 K
σ_{xx} (e^2/h)
σ_{xy} (e^2/h)

Figure 4

Supporting Information

Insulator-quantum Hall transition in monolayer epitaxial graphene

Lung-I Huang[ab], Yanfei Yang[ac], Randolph E. Elmquist[a],
Shun-Tsung Lo[*d], Fan-Hung Liu[d], and Chi-Te Liang[*bde]

[a]*National Institute of Standards and Technology (NIST), Gaithersburg, MD 20899, USA*
[b]*Department of Physics, National Taiwan University, Taipei 106, Taiwan*
[c]*Department of Physics, Georgetown University, Washington, DC 20057, USA*
[d]*Graduate Institute of Applied Physics, National Taiwan University, Taipei 106, Taiwan*
[e]Geballe Laboratory for Advanced Materials (GLAM), Stanford University, Stanford, CA 94305, USA

*shuntsunglo@mail.ncku.edu.tw and ctliang@phys.ntu.edu.tw

Sample preparation and measurements

Epitaxial graphene (EG) is formed after decomposition and Si sublimation on the surface of SiC at high temperatures. Angle-resolved photoelectron spectroscopy shows that newly-grown samples measured *in situ* have carrier concentrations $n \approx 10^{13}$ cm^{-2}, ascribed to charge-transfer from an insulating graphene-like buffer layer that is covalently bonded to the SiC substrate.[1] In order to study the electronic transport with $|n| < 10^{12}$ cm^{-2}, electrostatic[2, 3] or photochemical[4] gating through an insulating dielectric, molecular doping[5] directly on the EG surface, or atomic intercalation[1, 6] beneath the buffer layer have been used to modify the carrier concentration. In order to achieve low density EG, Our EG devices were fabricated utilizing a clean lithography process[7] that leaves the surface free of resist residues. After this fabrication process doping occurs due to or initiated by chemical etching of the protective layer and exposure to air, producing typical carrier densities of order $n \approx 10^{11}$ cm^{-2}. The devices can be cycled to higher or lower carrier density repeatedly by annealing at 70 °C to 150 °C or by air exposure, implicating oxygen and water molecules from the air as the source of p-type molecular doping.[8, 9]

Longitudinal resistivity ρ_{xx} was obtained by averaging the data from both sides of the conducting channel [voltage probes 1, 3 and voltage probes 1* and 3*] and Hall resistivity ρ_{xy} was measured across the central pair [2 and 2*] of device contacts [Fig. S1]. In graphene as well as in heterostructures, low carrier concentrations are often associated with percolating current paths that mix ρ_{xx} with ρ_{xy}. Data measured at both directions of the magnetic field were combined based on the recognized symmetries of the resistivity components to eliminate this mixing [10], which is strong in highly disordered samples for large values of ρ_{xx}.

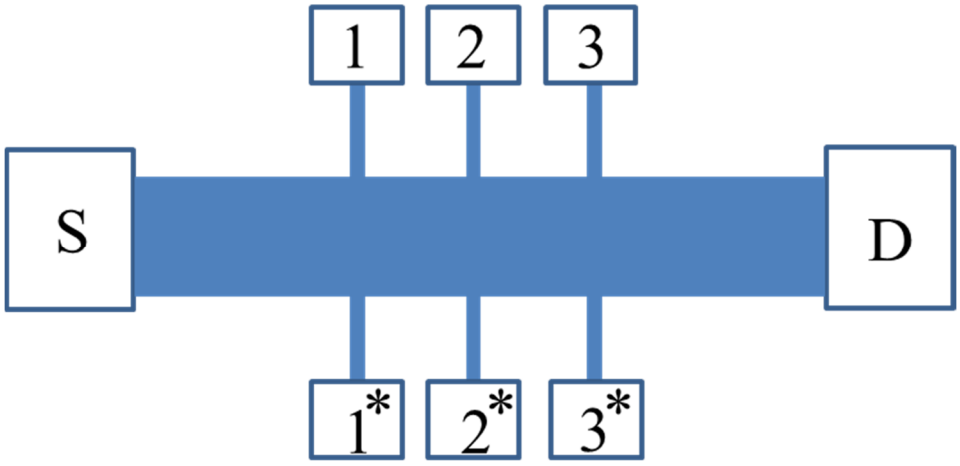

Figure S1 Schematic diagram showing a typical monolayer epitaxial graphene (EG) sample. S and D correspond to source and drain contacts. 1, 2, 3, 1^*, 2^* and 3^* are voltage probes. Channel dimensions, which are the same for all devices studied, are L = 0.6 mm, W = 0.1 mm, with voltage contacts spaced 0.1 mm apart along both sides of the device.

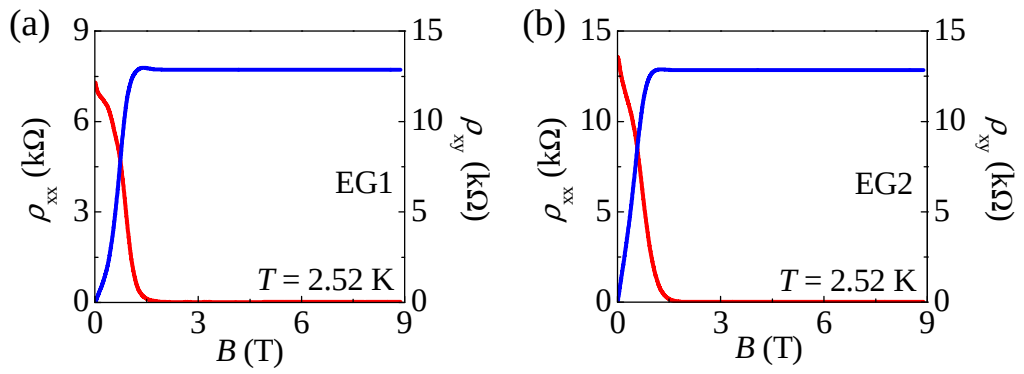

Figure S2. Resistivity values $\rho_{xx}(B)$ and $\rho_{xy}(B)$ of samples (a) EG1 and (b) EG2 for $0 < B < 9$ T.

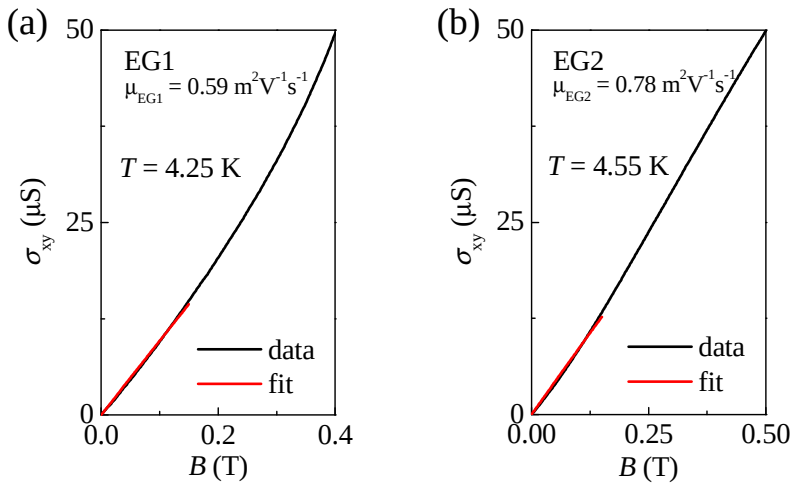

Figure S3 Determination of the mobility μ for samples (a) EG1 and (b) EG2 by fitting the measured σ_{xy} to $ne\mu^2B/(1+(\mu B)^2)$ over the range of $0 < B < 0.15$ T.

Weak localization and electron-electron interactions in our devices

In the weakly disordered regime, that is, the conductivity higher than $e^2/\pi h$, weak localization (WL) and electron-electron interaction (EEI) have significant contributions to the transport at low B in disordered graphene devices and may influence[11] the observed I-QH transitions.[12-16] The WL term modifies ρ_{xx} without affecting ρ_{xy}. The diffusive EEI has effects on both ρ_{xx} and ρ_{xy}. To investigate the observed I-QH transition, we have isolated the EEI contribution from the WL one following Ref. [17]. The EEI correction to the Drude conductivity[17] is given by

$$\delta\sigma_{xx}^{ee} = -K_{ee}G_0 \ln(\frac{\hbar}{k_B T\tau}), \quad (1)$$

where K_{ee} is an interaction parameter dependent on the type of sample and τ is the scattering time. This term gives a ln$T$ dependence to both σ_{xx} and to the Hall coefficient $R_H \equiv \delta\rho_{xy}(B, T)/\delta B$. The ln$T$ dependence of R_H is shown in Fig. S4 (a).

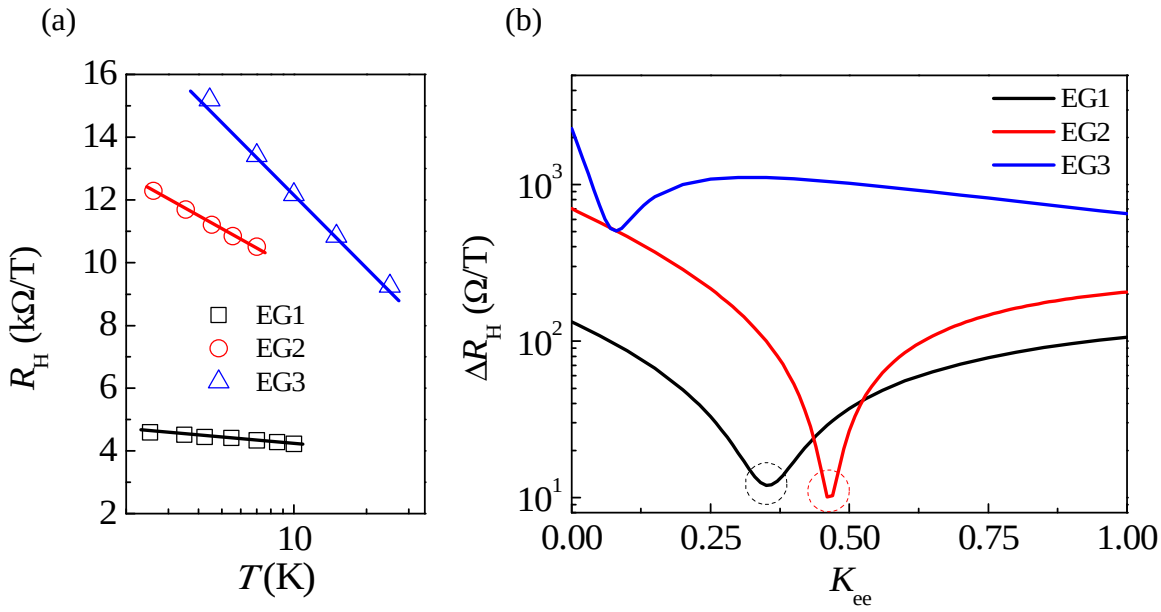

Fig. S4 (a) Uncorrected Hall slope $R_H \equiv \delta\rho_{xy}(B, T)/\delta B$ as a function of T. (b) Standard deviation of the corrected Hall slope at different T, $\Delta R_H = \sqrt{\frac{1}{N-1}\sum_i (R_H^i - \overline{R_H})^2}$ (where i runs over the measured temperature points), plotted against the interaction parameter K_{ee}. ΔR_H of the uncorrected data in (a) for each sample corresponds to $\triangle R_H(K_{ee} = 0)$ in (b).

According to Eq. (1), matrix inversion of the conductivity tensor shows that $\rho_{xx}(B,T)$ takes a parabolic form[18],

$$\rho_{xx} \approx \frac{1}{\sigma_D} - \frac{1}{\sigma_D^{\,2}}(1-\mu^2 B^2)\delta\sigma_{xx}^{ee}(T), \qquad (2)$$

for $\delta\sigma_{xx}^{ee} << \sigma_D$, where μ is the mobility, σ_D is the Drude conductivity and μ is the mobility. In addition, the EEI term gives a correction to the Hall coefficient $R_H \equiv \delta\rho_{xy}(B, T)/\delta B$ following $\delta R_H / R_H^0 = -2\delta\sigma_{ee}/\sigma_D$, where R_H^0 denotes the classical value of R_H [ref. 17]. The ln$T$ dependence of R_H is observed in Fig. S4(a), suggesting the influence of electron-electron interactions on the low-field insulating behavior.

Relevant to the data analysis, Eq. (2) indicates a T-independent point in ρ_{xx} at $\mu B = 1$. To clarify this its relation with the observed crossing issue, we remove the correction the contribution of EEI as described by Eq. (2) to ρ_{xx} at low B [ref. 18] and estimate the EEI strength following Ref. [17]. The correction $\delta\sigma_{xx}^{ee}$ described by Eq. (2) is subtracted from the measured σ_{xx} for with $0 \leq K_{ee} \leq 1$. By inverting the resulting conductivity tensor, we obtain a new corrected set of ρ_{xx} and ρ_{xy}. The optimum K_{ee} is identified when the standard deviation of the corrected R_H values at different T in Fig. S4(b) reaches its minimum. As shown in Figs. S5(a) and S5(c), for EG1 and EG2 the correction removal process renders the corrected ρ_{xy} insensitive to the change in T at low fields and the slope corresponds to R_H^0 without suffering from EEI. Most disordered device does not produce an optimum K_{ee} with reasonable confidence, and only a weak minimum (EG3) is obtained by this procedure. The T-independent points in $\rho_{xx}(B, T)$ survive in the corrected data for EG1 and EG2 and occur at only slightly lower crossing fields B_c^{ρ} after the correction [Figs. S5(a) and S5(b)]. The remaining T and B dependence of ρ_{xx} is attributed to WL effect (Supplementary Fig. S5), suggesting that the transition in EG1 and EG2 represents the crossover from WL to the $\nu = 2$ quantum Hall state. However, stronger disorder in EG3 whose low-T conductivity is lower than $e^2/\pi h$ makes the correction descriptions invalid.

Remove the corrections due to electron-electron interactions

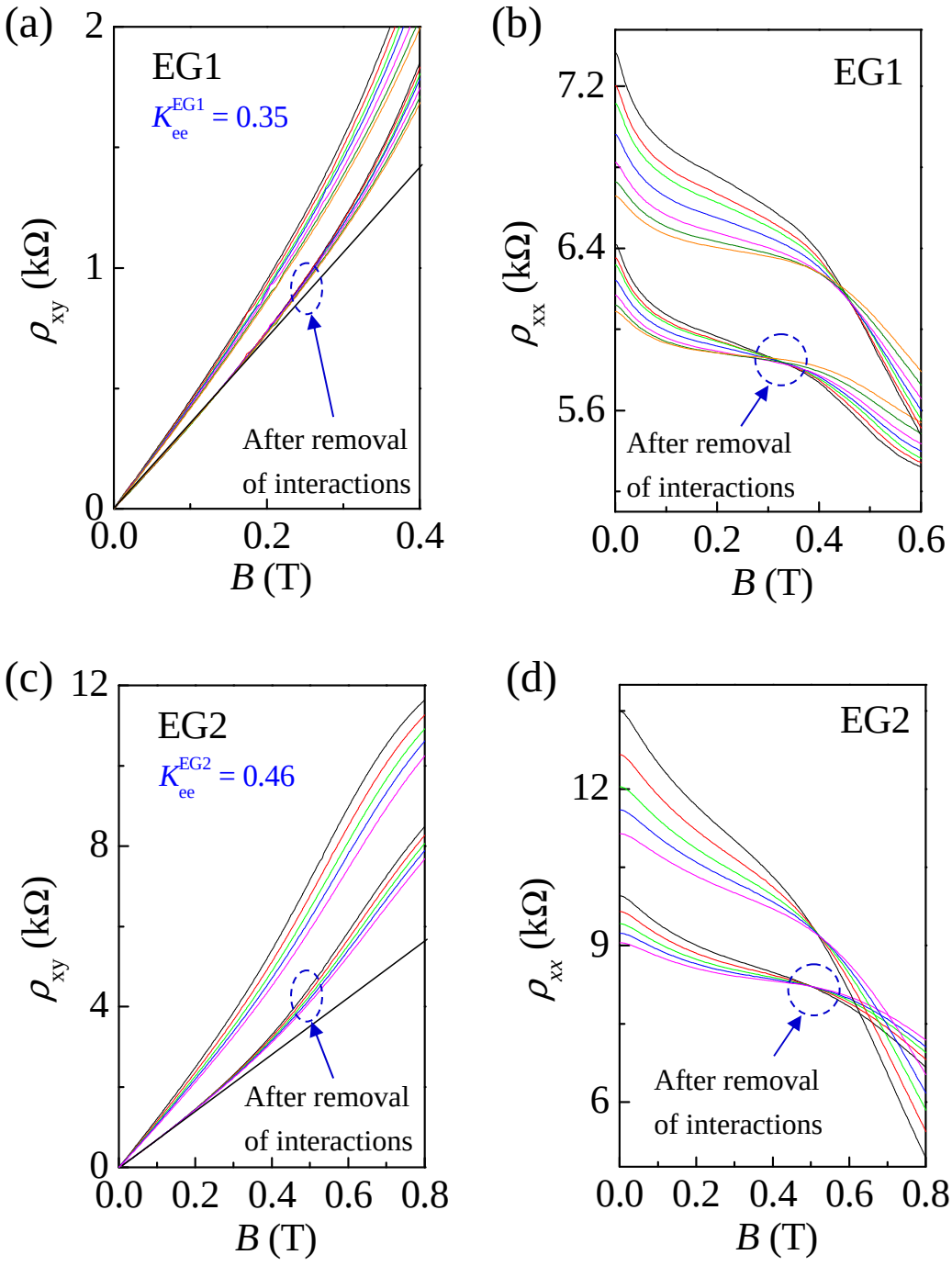

Fig. S5 Comparison of *T*-dependent resistivities for samples (a, b) EG1 and (c, d) EG2 before and after removal of interactions. The temperature ranges are the same as those given in the caption of Fig. 1.

Weak localization

Our experimental results can be fitted to the theoretical work of McCann *et al.*[19] as shown in Fig. S6 (a) and (b). We note that the WL effect contributes to a shift in σ_{xx} proportional to $\ln(\tau_\phi/\tau)$, where τ_ϕ is the phase relaxation time and approximately proportional to T^{-1} as shown in Fig. S6 (c); however, WL produces no contribution to Hall coefficient.

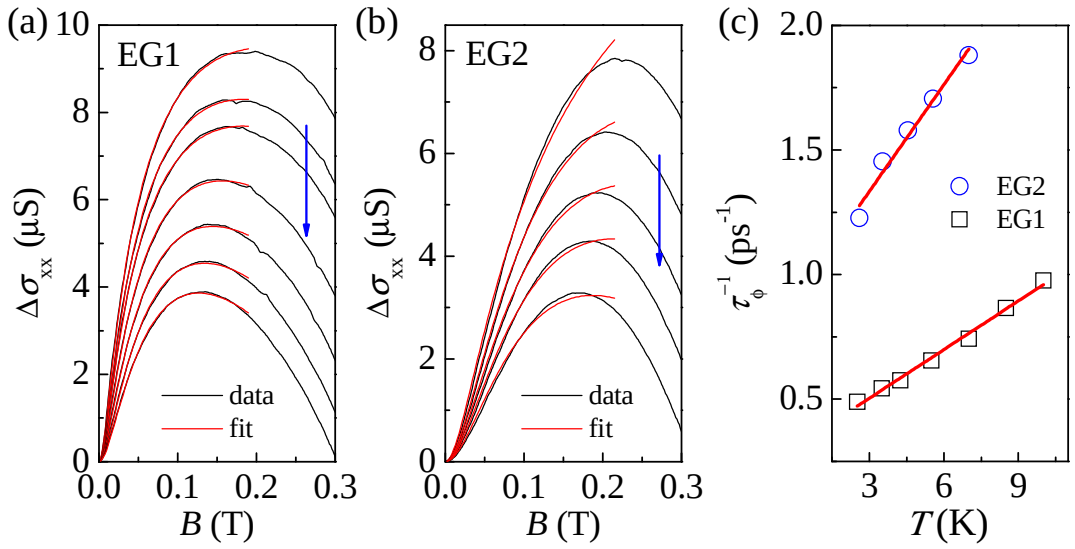

Figure S6 Fits of the measured $\Delta\sigma_{xx}(B) \equiv \sigma_{xx}(B) - \sigma_{xx}(B = 0)$ to the model developed by McCann *et al.* [19] for samples (a) EG1 and (b) EG2. The arrows indicate the temperature increase. (c) The decoherence rate τ_ϕ^{-1} obtained from the fits as a function of T.

Scaling of the Hall conductivity

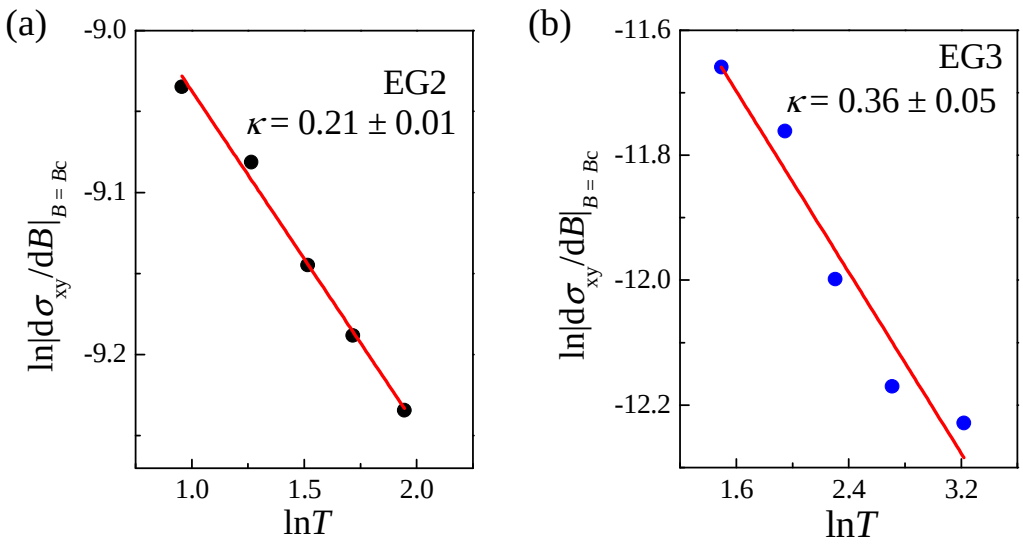

Figure S7 Fit of the slope of the transverse conductivity $d\sigma_{xy}/dB$ at the critical field B_c^{σ} to the power-law dependence on temperature T with an exponent κ for EG2 and EG3.

Table S1 Physical quantities of each EG sample.

Sample	Type	density (m^{-2})	K_{ee}	μ ($m^2V^{-1}s^{-1}$)	τ (fs)	Γ (meV)	μB_c^{ρ}
EG1	n	1.75×10^{15}	0.35	0.59	29	23	0.27
EG2	p	8.83×10^{14}	0.46	0.78	27	24	0.41
EG3	n	5.76×10^{14}	−	0.31	9	76	1.21

References

1. J. Ristein, S. Mammadov, and Th. Seyller, *Phys. Rev. Lett.* 2012, **108**, 246104.
2. D. B. Farmer *et al., Phys. Rev. B* 2011, **84**, 205417.
3. T. Shen *et al., J. Appl. Phys.* 2012, **111**, 013716.
4. S. Lara-Avila *et al., Adv. Mater.* 2011, **23**, 878-882.
5. C. Coletti *et al., Phys. Rev. B* 2010, **81**, 235401.
6. P. L. Levesque *et al., Nano Lett.* 2011, **11**, 132-137.
7. Y. Yang *et al., Small* 2015, **11**, 90-95.
8. S. Ryu *et al., Nano Lett.* 2010, **10**, 4944-4951.
9. Z. H. Ni *et al., J. Raman Spectros.* 2010, **41**, 479-483.
10. M. Hilke *et al., Nature* 1998, **395**, 675-677.
11. M. Y. Simmons *et al., Phys. Rev. Lett.* 2000, **84**, 2489-2492.
12. S. H. Song *et al., Phys. Rev. Lett.* 1997, **78**, 2200-2203.
13. H. W. Jiang *et al., Phys. Rev. Lett.* 1993, **71**, 1439-1442.
14. R. J. F. Hughes *et al., J. Phys.: Condens. Matter* 1994, **6**, 4763-4770.
15. T. Wang *et al., Phys. Rev. Lett*. 1994, **72**, 709-712.
16. E. Pallecchi *et al., Sci. Rep.* **3**, 1791 (2013).
17. K. E. J. Goh, M. Y. Simmons and A. R. Hamilton, *Phys. Rev. B* 2008, **77**, 235410.
18. G. M. Minkov *et al., Phys. Rev. B* 2003, **67**, 205306.
19. E. McCann *et al., Phys. Rev. Lett.* 2006, **97**, 146805.